Bending Deformation of Multiple Aligned Plates Toward Coalescence Induced by Capillarity

Kosuke Takahashi, Takahiro Matsuo, Kazuaki Inaba, and Kikuo Kishimoto

Abstract— **Deformation induced by capillarity needs to be characterized appropriately to avoid unexpected collapse or to control self-assembly of fine structures. Nevertheless, even simple phenomena such as the pinching together of two plates require delicate instruments for observation. Our group proposed a simple experimental setup in which parallel plates separated by small gaps and fixed at their bottom ends were lowered into a liquid. Bending deformation of the plates caused by capillary rises between their inner surfaces was observed at the liquid surface. The experiments revealed that plates do not coalesce simultaneously, but in a sequence starting from pairs with the current smallest gap and with little influence of capillary rises in neighboring plates. After each pair of plates had coalesced, they behave as a single plate causing subsequent coalescences to occur in a similar manner. An analytical model based on this prescription is established to predict the deflection of plate pairs up until coalescence finishes. The effectiveness of the model was confirmed by accurately predicting the sequence of coalescence in multiple plates. Furthermore, it is presented that conditions required to avoid either coalescence in a pair of plates or complete coalescence of all plates can be determined by a non-dimensional parameter.**

Index Terms— **Analytical models, Electronics packaging, Etching, Microfabrication, Microfluidics, Surface tension**

I. Introduction

RECENT developments in the manufacturing industry regarding microelectromechanical system (MEMS) are fueling the appearance of complex designs in smaller and thinner products, the objective being to improve performance[1]–[3]. In these fine structures, surface effects become more significant whereas at macroscopic scales, they are usually negligible. For example, micro-pillar production in the wet-etching process causes unexpected deformations if capillary action is considered improperly[4], [5]. During the dissolution of the masking layers, liquid solutions flowing into the small spaces between solid surfaces might induce forces of attraction arising from capillarity[6], [7]. Nevertheless, if properly characterized, this capillary-induced coalescence may be utilized to self-assemble fine structures. It is possible to gather aligned micro-pillars to form complex regular patterns[8]–[11] and control the packing density of carbon nanotubes to produce efficient electronic devices[12]–[14].

However, the application of capillary-induced coalescence in manufacturing is still limited because it is associated with complex numerical approaches to solving the governing equations of the fluid–structure interaction. Capillary coalescence is an instability phenomenon that results from the force of attraction between two solid surfaces that narrows their gap and reinforces further deflection. Such deformations have been widely characterized by using rather small and pliant structures of plates or pillars to surely cause coalescence and collapse[15]–[23]. Dynamics of elasto-capillary, such as time to reach equilibrium state[24], evaporation rate[25], [26], and drain rate of liquid[27] have also been investigated. However, there have been few studies regarding precise measurement of the bending deformation from initiation to coalescence even though it is indispensable to prevent collapse of structures with high aspect ratio, or to control manipulation actuated by elasto-capillary[28]. Capturing the initiation of deformation is difficult because elasto-capillary is usually observed under restricted conditions of employed microscopes.

Our group proposed a simple experimental setup using mesoscale structures that barely cause capillary-induced deformation, to monitor the progressive bending of the plates[29], [30]. Two polymer plates of sub-millimeter scales are aligned in parallel with a fixed spacing at one end. When the pair are lowered gradually at a constant velocity into a container filled with liquid, the force of attraction acts only along the liquid column formed between the plates above the liquid surface. As the plate is immersed further, the gap between the plates becomes smaller by bending inward. Subsequently, a liquid column becomes higher and promotes further plate bending. Observations are facilitated with this setup because the liquid column remains in focus at the initial height of the liquid surface, and hence a conventional digital microscope can capture the progressive deformation precisely. In addition, deflections of plates measured by this experimental setup were successfully predicted by a non-dimensional parameter consisting of material properties and geometry variables, which was derived from minimum potential energy. It was found that deflections of plates under static conditions must be smaller than 1/3 of their initial gap. Once they exceed this critical value, the bending deformation is accelerated to make contacts. Based

"This work was supported by JSPS KAKENHI Grant No. JP15K17934."

Kosuke Takahashi is with the Division of Mechanical and Space Engineering, Hokkaido University, Sapporo, Japan (e-mail: ktakahashi@eng.hokudai.ac.jp).

Takahiro Matsuo was with the Department. of Mechanical Sciences and Engineering, Tokyo Institute of Technology, Tokyo, Japan. (e-mail: t.matsuot224@gmail.com).

Kazuaki Inaba is with the Department. of Transdisciplinary Science and Engineering, Tokyo Institute of Technology, Tokyo, Japan (e-mail: inaba@mech.titech.ac.jp).

Kikuo Kishimoto was with the Department. of Transdisciplinary Science and Engineering, Tokyo Institute of Technology, Tokyo, Japan (e-mail: kkishimoto@ocean.zaq.jp).

on the prediction, a condition to avoid capillary-induced coalescence of a pair of plates was established by utilizing this critical deflection.

In this study, our approach is extended to multiple aligned plates. It is observed that the complete coalescence of the plates does not occur all at once, but in turn starting from a pair of thinner plates with the smallest gap. Therefore, the proposed non-dimensional parameter is still effective by focusing on pairs of plates with reconfigurations of thickness and gap between plates as the coalescence of plates proceeds. The bending deformation of multiple aligned plates is carefully observed from initiation to coalescence and compared with prediction by our analytical model.

II. EXPERIMENTAL

A. Experimental setup and material parameters

The polystyrene plates, the thickness w being of sub-millimeter scale, have the appropriate stiffness to be able to observe the capillary-induced coalescence by a conventional digital camera. The specimen consists of n plates of length L and depth b are fixed at one end with their gaps being D_i (i = 1, 2, …, n-1) [Fig. 1(a)]. It is connected to a linear actuator situated above the container, which is filled with liquid. It is then gradually lowered into the liquid at a constant velocity V. When the fixed end of the plates reaches the liquid surface, a liquid column is formed through capillary action in the small gap between plate surfaces, and the deflections of the plates y, become larger as the capillary rise increases by lowering further. Finally, complete coalescence is attained when the gap between the plates is filled with liquid by a contact at the tip of the plates. The gap observed at the liquid surface does not necessarily close completely [Fig. 1(b)].

In this study, the container was filled with silicone oil (Shinetsu KF-96-30cs). Surface energy, density, and kinematic viscosity are γ_{LV} = 20.2 mJ/m^2, ρ = 960 kg/m^3, and ν = 30 mm^2/s, respectively. Specimens consisting of multiple plates aligned in parallel were created by polystyrene cut to lengths L = 70 mm and 100 mm, depth b = 30 mm, and thickness w = 0.5 mm. The elastic modulus of the plate is E = 2.69 GPa. The contact angle of silicone oil was measured in our previous study, θ = 2.6°, using a Contact Angle Meter ECA-1 (Kyowa Interface Science Co., Ltd.)[29].

Three plates and five plates were aligned unevenly with spacings shown in Table 1. Specimen (3-i) and (3-ii) of three plates were prepared to confirm that the coalescence occurs at the smaller gaps and examine the influence of neighboring plate. Specimen (5-i) and (5-ii) of five plates were designed to observe the interaction of attracting pairs. The smaller gaps of 0.3 mm are separated for specimen (5-i) whereas three plates in the middle are evenly spaced for specimen (5-ii). Before immersing them into liquid, their actual distribution of initial spacings along their length were measured from images taken using a digital camera (Canon EOS 6D) to consider the plate waviness. Each specimen was then gradually immersed into the silicone oil from the fixed end at a constant velocity of V = 0.5 mm/s. The capillary rise and the plate deflections were recorded until the plates were completely submerged. The gaps between plates at the liquid surface were measured in terms of plate length under liquid l from images captured every five seconds (i.e., every 2.5-mm displacement of the specimen in the liquid). The accuracy of the measured gaps was confirmed by repeated experiments conducted under the same conditions imposed in our previous study[29].

B. Results

A sequence of images was taken of specimen (3-i), from when the fixed end entered the liquid surface (l = 0) [Fig. 2(a)]. The first coalescence, occurring for the pair of plates with the smaller gap, was barely affected by the presence of the other plate because the capillary rise for a smaller gap was higher and generated a stronger attraction [Fig. 2(b)–(d)]. Meanwhile, the capillary rise at the wider gap remained constant in height at h = 3.75 mm, measured by the arrow in Fig. 2 (b). This first coalescence, observed at l = 30 mm, widened the other gap and lowered the capillary height. On the coalescence, the plates were regarded as unified, and the resultant configuration now observed with the remained pair of plates corresponds to plate thicknesses of 2w and w. The height of the capillary rise remained lowered, but started to increase again at around l = 60 mm [Fig. 2(e)] and coalescence completed till l = 90 mm [Fig. 2(f)–(h)].

From the images taken from specimen (3-ii), the first coalescence of a pair occurred soon after the fixed end entered the liquid surface, at l = 5.0 mm to 10.0 mm [Fig. 3(a)–(c)], because the spacing between the plates was smaller. After the first coalescence, the bending of plates was similarly delayed as observed for specimen (3-i) because of the widened gap and doubled thickness of the unified plate. The second coalescence was confirmed till l = 45 mm [Fig. 3(d)–(h)].

The sequence of images captured from specimen (5-i), beginning at l = 0 [Fig. 4(a)], clearly showed the deflections of the plates at the smaller 0.3-mm gaps as soon as the plates began to be immersed [Fig. 4(b)–(c)]. Since the first coalescence occurred simultaneously at gaps D_2 and D_4, external meniscus formed on a plate at the right end was confirmed to be similarly negligible as neighboring capillary rises. The gap on the left side of D_1 became slightly smaller than that on the right side of D_3 because the plate thickness on the left end remained single and more pliant than the unified plates. The remaining single plate finally approached the right and the thickness trebled at l = 40 mm [Fig. 4(d)–(f)]. Further coalescence at D_3 was not observed until the entire specimen was submerged [Fig. 4(g)–(h)].

From the sequence of images captured from specimen (5-ii), coalescence in the 0.3-mm gaps D_2 and D_3 did not occur simultaneously in this case [Fig. 5(a)–(c)] because the center plate is located at an unstable position sandwiched by gaps of equal size. Hence, slight variations determine in which direction the plate moves. After a few moments, the second coalescence occurred in the center because the gap is smaller than the others [Fig. 5(d)]. The third coalescence was observed at D_4 [Fig. 5(f)] even though the axis of symmetry shifted slightly toward the left from the first unstable coalescence. This

is because the initial gap of D_4 was smaller than D_1 due to initial variation of the plate waviness. Coalescence of all the plates was eventually confirmed till l = 60 mm [Fig. 5(g)–(h)], whereas specimen (5-i) did not completely coalescence. It was found that the plate length enough to attain complete coalescence of all plates depends on the arrangements of the gaps even when the sum of the gap spacings is equal.

III. ANALYTICAL MODELS

A. Extension of symmetrically aligned two plates to those of different thicknesses

Our group proposed a symmetric analytical model for a pair of plates with a gap of D_0 under static conditions, and found a critical deflection of plates above which the bending deformation is accelerated to make contacts[29]. This critical deflection becomes unclear at higher immersion velocities, but V = 0.5 mm/s was confirmed to be slow enough to capture it [30]. Viscous effects are neglected in this study to focus on the extension of our static model to multiple plates.

The potential energy of a pair of plates can be expressed as a sum of the surface energy U_S, the gravitational potential energy of the liquid column U_g, and the elastic energy of plates U_b,

$$U = U_s + U_g + U_b$$

$$U_s = -2bh\gamma_{LV}\cos\theta + \{\pi(D_0/2 - y) - D_0\}b\gamma_{LV}$$

$$U_g = \frac{\rho g(D_0 - 2y)bh^2}{2} \tag{1}$$

$$U_b = \frac{Ebw^3}{4l^3}y^2.$$

In our previous study, the surface energy of the interface between the inner plate surfaces and liquid column (first term in U_s) was taken into account, but it has been modified here to include changes in surface area on top of the capillary column. The liquid surface between the plates was assumed to be flat originally, but the meniscus naturally curves by the plate deflection. The corresponding increase in the surface energy is expressed as $(2d_s - D_0)b\gamma_{LV}$, where the length on top of capillary rise is $2d_s$. From Fig. 6, d_s can be estimated from the radius of curvature R and the central angle of the arc ψ, which is calculated from the contact angle θ and the angle of deflection ϕ,

$$d_s = R\psi = \frac{(D_0/2 - y)}{\cos(\theta - \phi)}\left(\frac{\pi}{2} - \theta + \phi\right) \approx \frac{\pi}{2}\left(\frac{D_0}{2} - y\right). \tag{2}$$

Here, θ - ϕ is regarded as negligibly small, considering a few degrees of contact angle and a much longer plate length than their gap.

As for the gravitational potential energy, the volume of the liquid column is simply assumed to be a product of the rectangular area of the liquid surface $(D_0 - 2y)b$ and height h. The elastic energy is obtained by replacing the Laplace pressure distributed over the inner plate surface by the concentrated force at the liquid surface by assuming a much longer plate length l than the capillary height h.

The capillary height and the deflection of the plate in a static state can be obtained by applying conditions,

$$\frac{\partial U}{\partial h} = 0, \qquad \frac{\partial U}{\partial y} = 0. \tag{3}$$

By considering the plate deflection, the capillary height is

$$h = \frac{2\gamma cos\theta}{\rho g(D_0 - 2y)}. \tag{4}$$

Eliminating h from two simultaneous equations in Eq. (3) derives a relationship between the non-dimensional deflection $Y^* = 2y/D_0$ and the aspect ratio l/w for the plate immersed in the liquid,

$$\frac{1}{8}Y^*\left\{1 - \frac{2\alpha}{Y^*}\left(\frac{l}{w}\right)^3\right\}(1 - Y^*)^2 = \beta\left(\frac{l}{w}\right)^3, \tag{5}$$

where

$$\alpha = \frac{2\pi\gamma_{LV}}{ED_0}, \qquad \beta = \frac{2(\gamma_{LV}\cos\theta)^2}{E\rho g D_0^3}. \tag{6}$$

Our previously proposed non-dimensional number K for a pair of plates with the same thickness is derived on setting α = 0, and $D_0 = 2d_0$ [29], but it is redefined here as K^* for an extension to plates of different thicknesses

$$\frac{1}{8}Y^*(1 - Y^*)^2 = \beta\left(\frac{l}{w}\right)^3 \equiv K^*. \tag{7}$$

Since α originated from changes in surface area on top of the capillary column, the assumption α = 0 is effective when the effect of surface tension at top of the capillary column is small compared to the Laplace pressure considered in β. The α term may not be neglected at small gaps of plates, but the effect becomes smaller as the coalescence of plates proceeds due to enlarged gaps of D_0. Compared to the sensitivity of D_0, the contact angle has little influence on β as long as the wettability is good enough. Contact angles of $\theta < 10°$ would cause variations of β by only 3%.

Our model for symmetrically aligned plates can be applied to multiple plates by focusing only on the pair of adjacent plates that is pliant and with the smallest gap. After a pair of plates making contact, the plates act as a single plate with double the thickness and enlarged gap to the adjacent plates, followed by the next focus on the current pair of pliant plates with the smallest gap.

For a pair of plates with different thicknesses, the total deflection is a sum of plate deflections, $Y = y_1 + y_2$ (Fig. 7).

$$Y = \frac{4l^3}{Eb}\left(\frac{1}{w^3} + \frac{1}{(cw)^3}\right)P. \tag{8}$$

Here, the difference in the plate thicknesses is represented by their ratio $c \geq 1$. The elastic energy in Eq. (1) is modified by

introducing c and redefining α and β in Eq. (6), so that Eq. (5) and Eq. (7) are extended to asymmetric pairs of plates

$$\alpha = \frac{\pi\gamma_{LV}}{ED_0}\left(1+\frac{1}{c^3}\right), \qquad \beta = \frac{(\gamma_{LV}\cos\theta)^2}{E\rho g {D_0}^3}\left(1+\frac{1}{c^3}\right). \tag{9}$$

The relationship between Y^* and K^* in Eq. (7) is shown in Fig. 8. The bending deformation is accelerated to make contacts when $K^* > 1/54$ because the broken line corresponds to the local maxima of the potential energy obtained from Eq. (3). In other words, Y^* must be smaller than the critical deflection of $Y^* = 1/3$ if plate contact is to be avoided.

B. Application of K to multiple plates aligned with arbitrary gaps*

Now, the prediction of capillary-induced coalescence of plates by non-dimensional number K^* is applied to n (≥ 2) plates aligned with arbitrary gaps. The pairs of plates attracting with each other can be specified by the higher values of K^* and treated as a single plate by summing their thicknesses and enlarging the gap to neighboring plates. However, attracting pairs of plates cannot be specified for plates of uniform thickness aligned by uniform gaps because K^* is equal to all the pairs. In this case, attracting pairs are determined almost randomly, or by slight variation of the dimensions, due to instability. In addition, the process to complete coalescence depends on the patterns of attracting pairs. For example, focusing on 4 plates of the thickness w aligned by the uniform gaps D_0 shown in Fig. 9, there are two possible patterns of coalescence. One pattern forms two attracting pairs in the first coalescence, followed by coalescence of plates of the thickness $2w$ with their gap $2D_0$. The other pattern forms the attracting pair in the middle, followed by coalescence of the plate of thickness $2w$ and the plate of thickness w in either left or right side. The plate of thickness of $3w$ finally attracts to the remaining one of thickness w. Comparing these two patterns, the latter pattern causes the coalescence more easily because the thickness of one plate in the pair is w, whereas both thicknesses of the pair are $2w$ in the former one, whose bending stiffness is 8 times higher. Therefore, the complete coalescence occurs the most unlikely when accumulated coalescence results in equal thickness of the unified plates as the last pair. In other words, all the plates certainly coalescence to unify if the non-dimensional number K^* of this last pair ($c = 1$) is greater than 1/54.

This concept can be also applied to the plates of various thicknesses aligned with various gaps by representing their average thickness and gap,

$$\overline{D_0} = \frac{1}{n-1}\sum_{i=1}^{n-1} D_i\,, \qquad \overline{w} = \frac{1}{n}\sum_{i=1}^{n} w_i\,. \tag{10}$$

When the coalescences are accumulated to form unified plates of the equal thickness as the last pair, the thickness and the gaps between them are expressed by $n\overline{D_0}/2$ and $n\overline{w}/2$, respectively. As a result, a condition required to cause complete coalescence of multiple plates is derived as

$$\frac{1}{6912} < \frac{1}{n^6}\frac{(\gamma_{LV}\cos\theta)^2}{E\rho g\overline{D_0}^3}\left(\frac{l}{\overline{w}}\right)^3 \equiv K_n^*. \tag{11}$$

IV. MODEL VALIDATIONS

A. Capillary-coalescence of multiple plates by updated pairs

The progress toward plate coalescence obtained from the experimental results were compared with the analytical solution. Initially, the height of the capillary rise observed from specimen (3-i) was compared with the analytical solution in static conditions of Eq. (4), giving $h = 3.83$ mm. The deviation from the height of 3.75 mm, measured by the arrow in Fig. 2 (b), is less than 3%, so that the velocity of immersion $V = 0.5$ mm/s is confirmed to be slow enough.

The gaps between the three plates of specimens (3-i) and (3-ii) as measured from camera images are presented in terms of the aspect ratio l/w for the plate under liquid, in Fig. 10 (a) and (b). The first contact between two single-thickness plates (red markers) are compared with results from the analytical model with $c = 1$ (red curve), Eqs. (5) and (9). The second contact (blue markers) between a single plate and a doubled plate are compared with results from the analytical model with $c = 2$ (blue curve), Eqs. (5) and (9). Recall that the broken lines correspond to local maxima of the potential energy, and hence the plate deflections increase rapidly to make contacts after the critical deflection $Y^* = 1/3$ is surpassed.

For specimen (3-i), the plates with the smaller gap of $D_0 = D_1 = 0.5$ mm are the first to deflect; the other plate can be neglected. The increase in the sum of the plate deflections Y^* corresponds well to the analytical solution of $c = 1$. When the experimental result for Y^* exceeds its critical deflection of 1/3 at around $l/w = 50$, the increment in the deflection, which was measured every five seconds, becomes larger indicating an accelerated growth in bending deformation. The increments become smaller again once the tip of plate has made contact [Fig. 1(b)]. With coalescence completed at around $l/w = 60$, the other gap was reconfigured to $D_0 = D_2 + D_1/2 = 1.25$ mm, assuming that the first coalescence occurred in the middle of gap D_1. The analytical solution of $c = 2$ was then compared with the experimental results, and it also corresponded well. The open makers of D_2, showing increase in the gap during the first coalescence in the gap D_1, are ignored here. Furthermore, the larger increment generated by the accelerated bending deformation complete coalescence was clearly observed around $l/w = 150$, where the experimental results surpass the critical deflection.

As for specimen (3-ii), complete coalescence occurred first in the smaller gap of $D_1 = 0.3$ mm. Compared with specimen (3-i), the first coalescence was observed at a smaller l/w value as expected from the smaller initial gap. In addition, the measured deflections were slightly larger than the analytical solution of $c = 1$, and their increments were rather large from the beginning. These results indicate that an accelerated bending deformation was initiated at a lower capillary height than for the analytical solution. Because the analytical model assumes the force of attraction is concentrated at the liquid surface to simplify the

calculation of the elastic energy, there is a discrepancy with the results of experiments when the aspect ratio l/w for the plate under liquid is insufficient compared with the capillary height. Following the first complete coalescence, the other gap was reconfigured to $D_0 = D_2 + D_1/2 = 0.65$ mm, for which the analytical solution corresponded well with the experimental results. The plate under liquid l/w became sufficiently long to regard the force of attraction as being concentrated. The accelerated bending deformation was also clearly observed with large increments at around $l/w = 80$ when the experimental results exceed the critical deflection.

The results obtained from experiments with the five-plate specimen are also compared with the analytical solutions [Fig. 11(a) and (b)]. The increase in gap spacing resulting from the coalescence in other gaps (open markers in Fig. 10) is not shown here to focus solely on the attracting pair of plates.

As for specimen (5-i) [Fig. 11(a)], the plate deflections corresponding to the smaller gaps $D_2 = D_4 = 0.3$ mm almost commenced simultaneously with the two pairs proceeding toward plate coalescence. The deflections measured in the experiments were slightly larger than the analytical solution with $D_0 = 0.3$ mm and $c = 1$, as observed in the first coalescence of specimen (3-ii). After the coalescence, D_1 and D_3 were reconfigured to $D_0 = 0.65$ mm and 0.8 mm, respectively, with plate deflections commencing next for the smaller D_1 gap. The deformation corresponded well with the analytical solution [Fig. 11(a); blue markers and curve]. Accelerated bending deformation as indicated by the large increments was also observed around $l/w = 70$, corresponding to the critical deflection. Gap D_3 did not close until the entire specimen was submerged, but the increases in the deflection roughly followed that from the analytical solution.

As for specimen (5-ii) [Fig. 11(b)], the center plate was deflected into gap D_2 in accordance with the analytical solution, but could have been deflected the other way, as described for Fig. 5. After the first coalescence, gaps D_1 and D_3 were reconfigured to $D_0 = 0.65$ mm and 0.45 mm, respectively. The second coalescence at gap D_3 also followed the analytical solution well. However, the deformations associated with the third coalescence at gap D_4 and the fourth coalescence at D_1 deviated from the analytical solutions. As described in Fig. 5(f), the third coalescence was not supposed to occur at D_4, but D_1 because the center plate was directed to the left at the first coalescence. The smaller initial gap at D_4 rather than that at D_1 caused the deviation from the prediction for the reconfigured gaps. The coalescence of plates is an instability phenomenon above the critical deflection, so that variations in the experiment is sensitive to plate waviness, which accumulates as the coalescence of plates proceeds. The deviation from experimental results, caused mainly by plate geometry, is expected to become smaller in actual MEMS devices because they have more precise dimensions. Further investigations though are required. Nevertheless, significant increases in Y^* were still observed for both third and fourth coalescences as the critical deflection is approached. Therefore, the analytical solution can predict the initiation of the accelerated bending deformation during contact and is useful in determining the amount of plate deflection possible while also avoiding coalescence.

B. Evaluation by proposed non-dimensional number

If α in Eq. (9) is negligible, the non-dimensional deflection Y^* is uniquely determined from the non-dimensional parameter K^*. The experimental results of Y^* (Figs. 10 and 11) were replotted in terms of K^* by substituting l/w into Eq. (7) for the three-plate and five-plate specimens [Fig. 12(a) and (b)]. Note that the results obtained during the first coalescence were discarded here because the analytical model is ineffective as the capillary height is too high to assume the force of attraction is concentrated. The solid lines in Fig. 12 represent Eq. (7); the extended broken lines are solutions of the local maxima of the potential energy, which were neglected when comparing with the experimental results.

For the three-plate specimens (3-i) and (3-ii), the K^* dependence of the deflections Y^* during the second coalescence is similar and closely matches the analytical model. An accelerated bending deformation is also clearly observed from both these specimens near the turning point of the analytical solution, which corresponds to a local maximum at $(K^*, Y^*) = (1/54, 1/3)$. Thus, after the first coalescence, neglecting α is confirmed to be effective in predicting the plate deflection using K^*. For the five-plate specimens (5-i) and (5-ii), the variation in Y^* as a function of K^* is larger compared with that for the three-plate specimens. Nevertheless, they can be regarded as being almost identical by considering the different thicknesses of plates and gaps during each coalescence. The approximate behaviors during deflection are similar in all results; Y^* increases barely at the beginning, gradually towards $Y^* = 1/3$, and rapidly to make contacts once the value passes the critical deflection. Despite the simple reconfigurations of thickness and gap after each coalescence, the progress towards coalescence for both the three-plate and five-plate specimens can be predicted by the non-dimensional parameter K^*.

The non-dimensional parameter K^*_n in Eq. (11) for the three-plate specimens (3-i) and (3-ii) are 1.97e-4 and 1.30e-3, respectively, when the length of plate in liquid is $l = 70$ mm. Because they are both greater than $1/6912 \simeq 1.45\text{e-}4$, all three plates coalescence. For the five-plate specimens, the non-dimensional parameter of $K^*_n = 1.31\text{e-}5$ for both specimens (5-i) and (5-ii), calculated from the average gap between plates, is smaller than 1/6912, corresponding to the result that specimen (5-i) did not cause complete coalescence. Complete coalescence was observed in specimen (5-ii) because each process of coalescence had a pliant single plate, as explained in the latter case in Fig. 9.

V. CONCLUSIONS

Capillary-induced bending of multiple aligned plates with various gap spacings was observed in detail from its initiation to plate contact by immersing them into silicone oil. As a result, coalescence was found to occur individually and sequentially, so that the deflection of plates is predictable by reconfiguring the plate thicknesses and the gap spacing each time coalescence occurs and focusing on the pair of pliant plates with the current smallest gap.

A non-dimensional parameter was redefined as K^* for a pair of plates with different thicknesses to predict the plate deflection based on our previous study which proposed an analytical

model for a pair of identical plates. The non-dimensional parameter K^* was confirmed to be effective particularly in capturing the initiation of accelerated bending deformation toward coalescence at Y^* (plate deflections normalized by their original gap) = 1/3 is precisely predicted. Therefore, plate coalescence cannot be prevented if pairs of plates satisfy $K^* > 1/54$. Note that the discrepancy between the analytical solution and experimental results is nonnegligible when the aspect ratio l/w of the plate under liquid is rather small compared with the capillary height.

In addition, it was found that patterns of prior coalescences affect the following ones and determine whether complete coalescence of all plates occurs. The most unpreferable pattern that induces coalescence of all the plates is the equally grouped plates for the last pair through previous coalescences. Therefore, the condition of $K^* > 1/54$ using the average thickness and gap of the n aligned plates led to the required conditions for complete coalescence of all the plates as the non-dimensional parameter $K^*_n > 1/6912$. The design of the fine structures that help to avoid collapse or to use self-assembly by capillarity can be managed with these non-dimensional parameters.

REFERENCES

[1] T. S. Arthur, D. J. Bates, N. Cirigliano, D. C. Johnson, P. Malati, J. M. Mosby, E. Perre, M. T. Rawls, A. L. Prieto, and B. Dunn, "Three-dimensional electrodes and battery architectures," *MRS Bull.*, vol. 36, no. 07, pp. 523–531, 2011.

[2] J. K. D. Berman, "Surface science, MEMS and NEMS: Progress and opportunities for surface science research performed on, or by, microdevices," *Prog. Surf. Sci.*, vol. 88, no. 2, pp. 171–211, May 2013.

[3] W.-M. Zhang, H. Yan, Z.-K. Peng, and G. Meng, "Electrostatic pull-in instability in MEMS/NEMS: A review," *Sensors Actuators A Phys.*, vol. 214, pp. 187–218, Aug. 2014.

[4] T. Tanaka, M. Morigami, and N. Atoda, "Mechanism of Resist Pattern Collapse during Development Process," *Jpn. J. Appl. Phys.*, vol. 32, no. Part 1, No. 12B, pp. 6059–6064, Dec. 1993.

[5] D. Chandra and S. Yang, "Stability of High-Aspect-Ratio Micropillar Arrays against Adhesive and Capillary Forces," *Acc. Chem. Res.*, vol. 43, no. 8, pp. 1080–1091, Aug. 2010.

[6] C. H. Mastrangelo and C. H. Hsu, "Mechanical stability and adhesion of microstructures under capillary forces. I. Basic theory," *J. Microelectromechanical Syst.*, vol. 2, no. 1, pp. 33–43, Mar. 1993.

[7] C. H. Mastrangelo and C. H. Hsu, "Mechanical stability and adhesion of microstructures under capillary forces. II. Experiments," *J. Microelectromechanical Syst.*, vol. 2, no. 1, pp. 44–55, Mar. 1993.

[8] S. H. Kang, N. Wu, A. Grinthal, and J. Aizenberg, "Meniscus Lithography: Evaporation-Induced Self-Organization of Pillar Arrays into Moiré Patterns," *Phys. Rev. Lett.*, vol. 107, no. 17, p. 177802, Oct. 2011.

[9] M. De Volder and A. J. Hart, "Engineering Hierarchical Nanostructures by Elastocapillary Self-Assembly," *Angew. Chemie Int. Ed.*, vol. 52, no. 9, pp. 2412–2425, 2013.

[10] Y. Hu, Z. Lao, B. P. Cumming, D. Wu, J. Li, H. Liang, J. Chu, W. Huang, and M. Gu, "Laser printing hierarchical structures with the aid of controlled capillary-driven self-assembly.," *Proc. Natl. Acad. Sci. U. S. A.*, vol. 112, no. 22, pp. 6876–81, Jun. 2015.

[11] S. H. Tawfick, J. Bico, and S. Barcelo, "Three-dimensional lithography by elasto-capillary engineering of filamentary materials," *MRS Bull.*, vol. 41, no. 02, pp. 108–114, Feb. 2016.

[12] E. J. García, A. J. Hart, B. L. Wardle, and A. H. Slocum, "Fabrication of composite microstructures by capillarity-driven wetting of aligned carbon nanotubes with polymers," *Nanotechnology*, vol. 18, no. 16, p. 165602, Apr. 2007.

[13] M. De Volder, S. J. Park, S. H. Tawfick, D. O. Vidaud, and A. J. Hart, "Fabrication and electrical integration of robust carbon nanotube micropillars by self-directed elastocapillary densification," *arXiv:1009.1592*, Sep. 2010.

[14] S. Tawfick, A. J. Hart, and M. De Volder, "Capillary bending of Janus carbon nanotube micropillars," *Nanoscale*, vol. 4, no. 13, pp. 3852–3856, Jun. 2012.

[15] H. Namatsu, K. Kurihara, M. Nagase, K. Iwadate, and K. Murase, "Dimensional limitations of silicon nanolines resulting from pattern distortion due to surface tension of rinse water," *Appl. Phys. Lett.*, vol. 66, no. 20, pp. 2655–2657, May 1995.

[16] K. Yoshimoto, M. P. Stoykovich, H. B. Cao, J. J. de Pablo, P. F. Nealey, W. J. Drugan, J. J. de Pablo, P. F. Nealey, and W. J. Drugan, "A two-dimensional model of the deformation of photoresist structures using elastoplastic polymer properties," *J. Appl. Phys.*, vol. 96, no. 4, pp. 1857–1865, Aug. 2004.

[17] H.-Y. KIM and L. MAHADEVAN, "Capillary rise between elastic sheets," *J. Fluid Mech.*, vol. 548, no. 1, p. 141, Feb. 2006.

[18] J. M. Aristoff, C. Duprat, and H. A. Stone, "Elastocapillary imbibition," *Int. J. Non. Linear. Mech.*, vol. 46, no. 4, pp. 648–656, May 2011.

[19] N. R. Bernardino and S. Dietrich, "Complete wetting of elastically responsive substrates," *Phys. Rev. E*, vol. 85, no. 5, p. 051603, May 2012.

[20] A. D. Gat and M. Gharib, "Elasto-capillary coalescence of multiple parallel sheets," *J. Fluid Mech.*, vol. 723, pp. 692–705, May 2013.

[21] C.-C. Chang, Z. Wang, Y.-J. Sheng, and H.-K. Tsao, "Nanostructure collapse by elasto-capillary instability," *Soft Matter*, vol. 10, no. 42, pp. 8542–8547, Aug. 2014.

[22] K. Singh, J. R. Lister, and D. Vella, "A fluid-mechanical model of elastocapillary coalescence," *J. Fluid Mech.*, vol. 745, no. 4, pp. 621–646, Apr. 2014.

[23] Z. Wei, T. M. Schneider, J. Kim, H.-Y. Kim, J. Aizenberg, and L. Mahadevan, "Elastocapillary coalescence of plates and pillars," *Proc. R. Soc. A Math. Phys. Eng. Sci.*, vol. 471, no. 2175, pp. 20140593–20140593, Jan. 2015.

[24] C. DUPRAT, J. M. ARISTOFF, and H. A. STONE, "Dynamics of elastocapillary rise," *J. Fluid Mech.*, vol. 679, pp. 641–654, Jul. 2011.

[25] Z. Wei and L. Mahadevan, "Continuum dynamics of elastocapillary coalescence and arrest," *EPL (Europhysics Lett.*, vol. 106, no. 1, p. 14002, Apr. 2014.

[26] A. Hadjittofis, J. R. Lister, K. Singh, and D. Vella, "Evaporation effects in elastocapillary aggregation," *J. Fluid Mech.*, vol. 792, pp. 168–185, Apr. 2016.

[27] D. Shin and S. Tawfick, "Polymorphic Elastocapillarity: Kinetically Reconfigurable Self-Assembly of Hair Bundles by Varying the Drain Rate," *Langmuir*, vol. 34, no. 21, pp. 6231–6236, May 2018.

[28] D. George, R. Anoop, and A. K. Sen, "Elastocapillary powered manipulation of liquid plug in microchannels," *Appl. Phys. Lett.*, vol. 107, no. 26, p. 261601, Dec. 2015.

[29] K. Takahashi, S. Sugita, S. Oshima, K. Inaba, and K. Kishimoto, "Evaluation of capillary-induced deformation of thin plates due to liquid column formation," *Appl. Phys. Lett.*, vol. 103, no. 4, p. 043113, 2013.

[30] K. Takahashi, T. Matsuo, M. Furuta, S. Oshima, K. Inaba, and K. Kishimoto, "Wetting-induced attraction of thin plates due to capillary flow," *Mech. Eng. Lett.*, vol. 2, no. 0, pp. 16-00227-16-00227, 2016.

Table 1 Initial gaps between aligned plates [mm]

Specimen	D_1	D_2	D_3	D_4
3-i	0.5	1.0	-	-
3-ii	0.3	0.5	-	-
5-i	0.5	0.3	0.5	0.3
5-ii	0.5	0.3	0.3	0.5

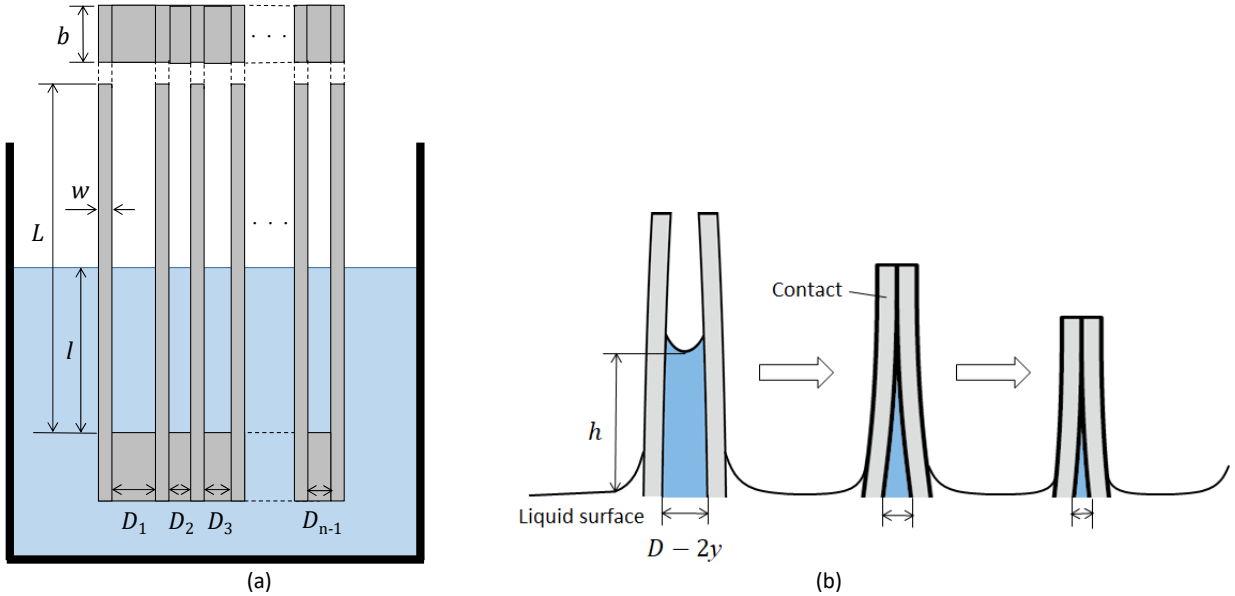

(a) (b)

Fig. 1. Schematic diagrams showing (a) the experimental setup to observe the capillary rise between a pair of plates and (b) the measured gap between plate pairs during plate deflection and plate contact after complete coalescence.

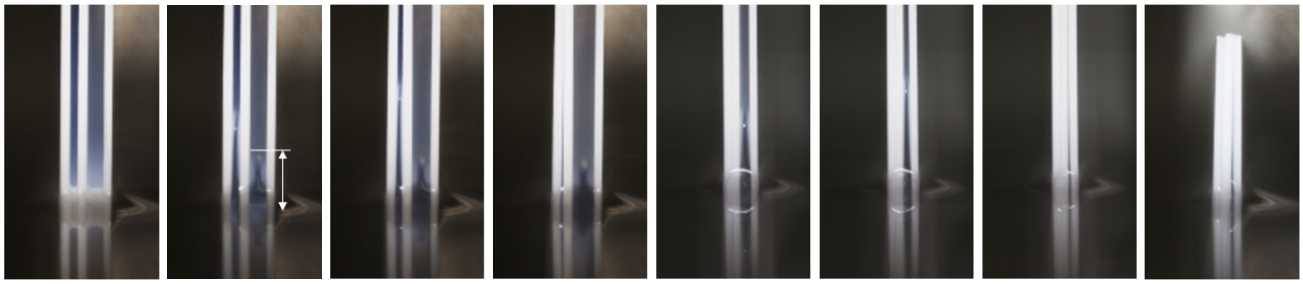

(a) l = 0 mm (b) l = 10 mm (c) l = 20 mm (d) l = 30 mm (e) l = 60 mm (f) l = 70 mm (g) l = 80 mm (h) l = 90 mm

Fig. 2. Deformation sequence of three plates aligned in parallel and the increase in capillary rises observed in specimen (3-i) from the beginning (a). A higher capillary rise is clearly observed at the smaller gap of 0.5 mm until plate coalescence at l = 10 mm (b), l = 20 mm (c), and l = 30 mm (d). The increase in capillary rise in the other gap of 1.0 mm is also clear at l = 60 mm (e), l = 70 mm (f), and l = 80 mm (g) until complete coalescence occurs at l = 90 mm (h).

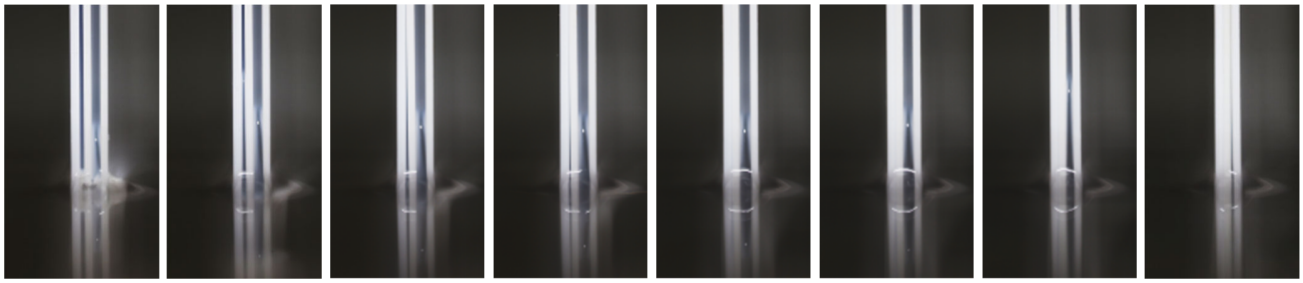

(a) l = 0 mm (b) l = 5.0 mm (c) l = 10 mm (d) l = 15 mm (e) l = 30 mm (f) l = 35 mm (g) l = 40 mm (h) l = 45 mm

Fig. 3. Deformation sequence of three plates aligned in parallel and the increase in capillary rises observed in specimen (3-ii) from the beginning (a). A higher capillary rise is clearly observed at the smaller gap of 0.3 mm until plate coalescence occurs at l = 5.0 mm (b), l = 10 mm (c), and l = 15 mm (d). An increase in capillary rise in the other gap of 0.5 mm is also clear at l = 30 mm (e), l = 35 mm (f), and l = 40 mm (g) until complete coalescence occurs at l = 45 mm (h).

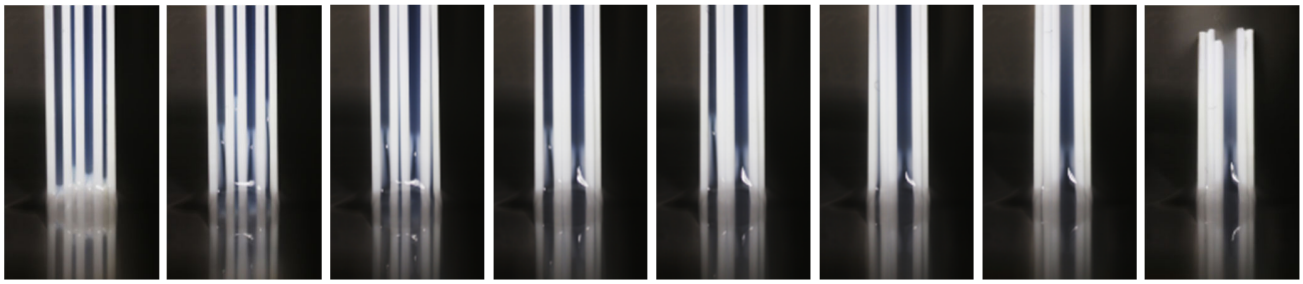

(a) l = 0 mm (b) l = 5.0 mm (c) l = 10 mm (d) l = 30 mm (e) l = 35 mm (f) l = 40 mm (g) l = 50 mm (h) l = 60 mm

FIG. 4. Deformation sequence of five plates aligned in parallel and the increase in capillary rises observed in specimen (5-i) from the beginning (a). A higher capillary rise is almost simultaneously confirmed at the smaller gap of 0.3 mm until coalescence occurs at l = 5.0 mm (b) to l = 10 mm (c). An increase in the capillary rise in the other gap of D_1 is also clearly observed at l = 30 mm (d), l = 35 mm (e), and l = 40 mm (f). Coalescence does not occur at gap D_3 until all plates are immersed as observed through l = 50 mm (g) to l = 60 mm (h).

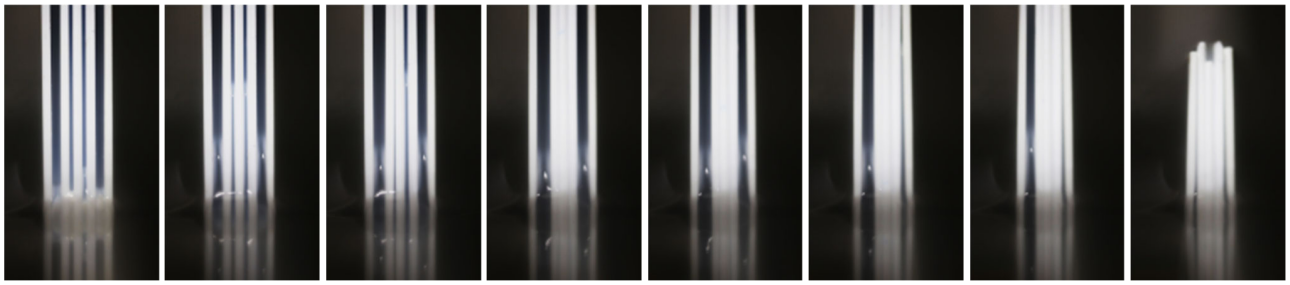

(a) l = 0 mm (b) l = 7.5 mm (c) l = 15 mm (d) l = 40 mm (e) l = 45 mm (f) l = 50 mm (g) l = 55 mm (h) l = 60 mm

FIG. 5. Deformation sequence of five plates aligned in parallel and the increases in capillary rises observed in specimen (5-ii) from the beginning (a). Higher capillary rises almost simultaneously increase in the smaller gaps of 0.3 mm as observed at l = 7.5 mm (b), but coalescence occurs in the gap of D_2 at l = 15 mm (c). Even though the initial arrangement of the plates is symmetric, the first coalescence towards the left breaks the symmetry and causes uneven capillary rises observed at l = 40 mm (d), and l = 45 mm (e). Coalescence at D_4 occurs earlier at l = 50 mm (f), and the remaining gap of D_1 eventually disappears as observed at l = 55 mm (g) and l = 60 mm (h).

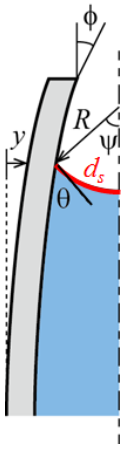

Fig. 6. Analytical model of the curvature on top of the capillary rise formed by plate deflection and contact angle between plate and liquid.

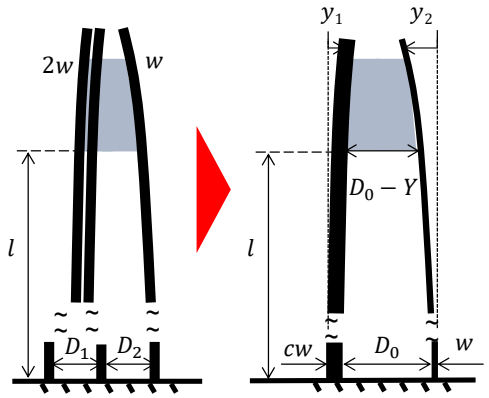

Fig. 7. Reconfiguring plate thickness and gap between plates after plate coalescence. The plate thickness doubles after coalescence at the D_1 gap of and the adjacent gap becomes $D_0 = D_2 + D_1/2$.

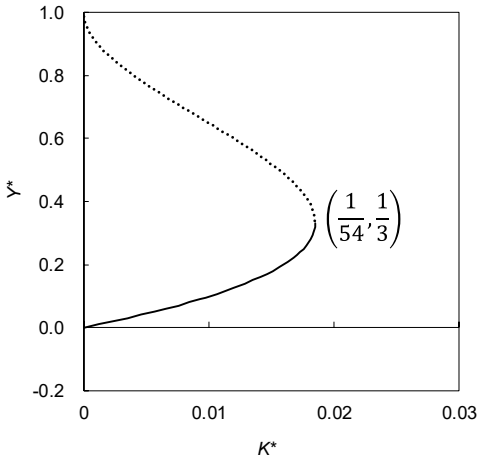

Fig. 8. Analytical solution of the relationship between deflections Y^* and the non-dimensional number K^*. An equilibrium state is obtained if the non-dimensional number is smaller than 1/54, but otherwise unstable deformations to contact occur.

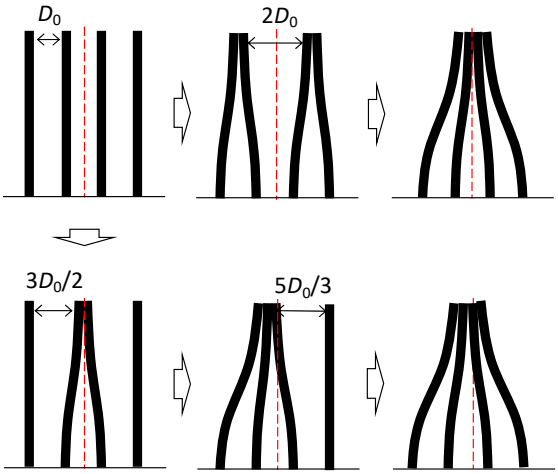

Fig. 9. Difference in the final appearance due to former processes of coalescence. The condition to complete coalescence of all the plates is the most difficult when the last pair is equally grouped (top), but it is easier if the pair of attraction includes thinner plate (bottom).

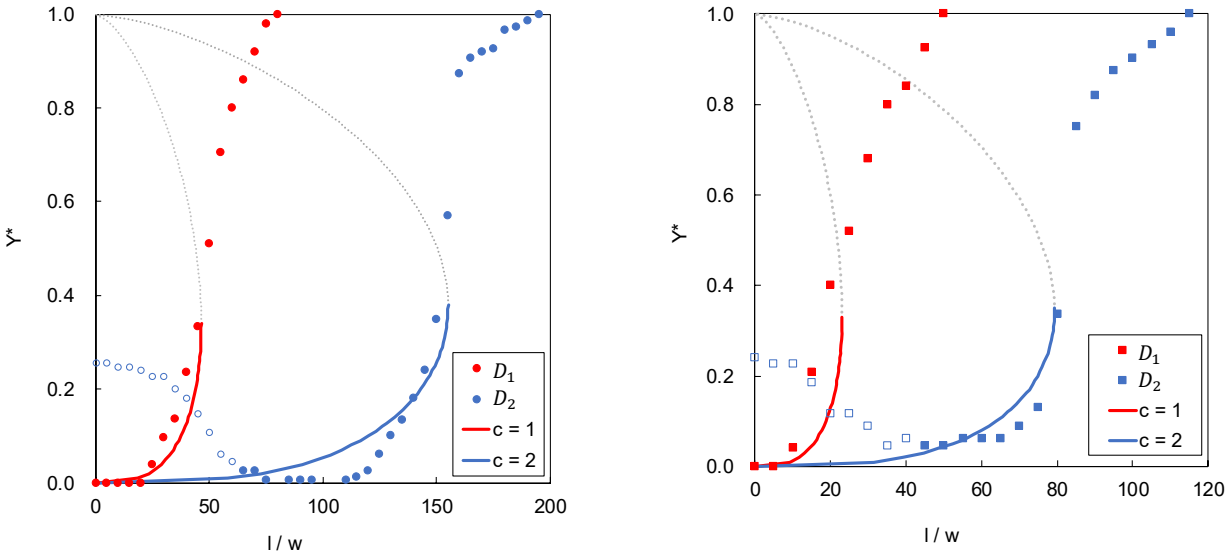

(a) D_1 = 0.5 mm, D_2 = 1.0 mm

(b) D_1 = 0.3 mm, D_2 = 0.5 mm

Fig. 10. Progressive deformation observed from three plates until the first and second contact obtained from specimens (3-i) and (3-ii), the gaps between plates being (a) (D_1, D_2) = (0.5 mm, 1.0 mm) and (b) (0.3 mm, 0.5 mm), respectively. Experimental results correspond well with the solid lines representing the analytical solution of Eq. (5).

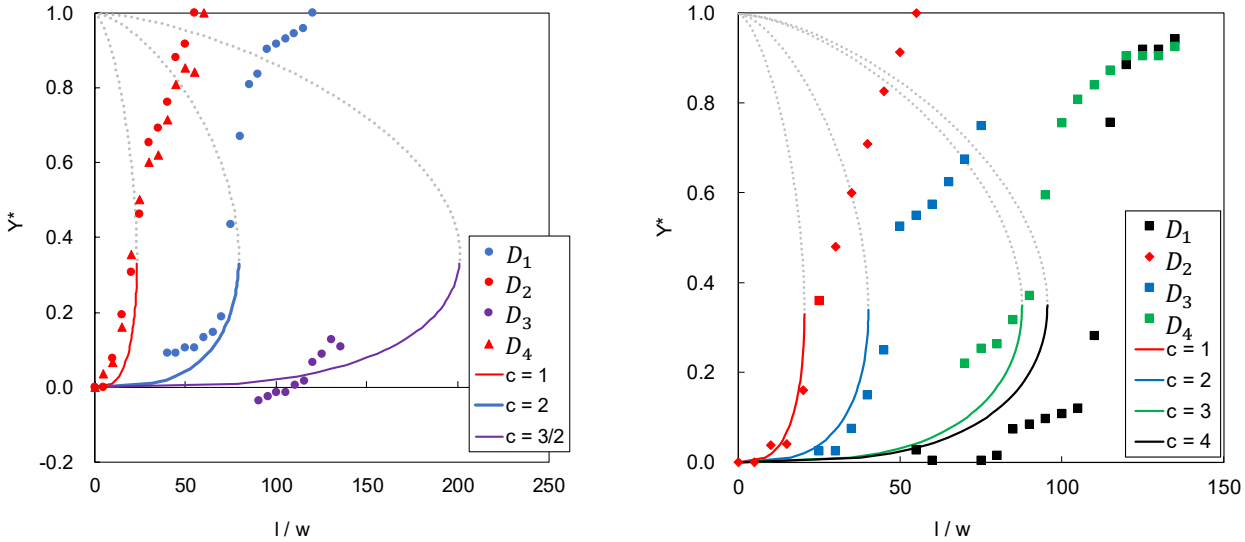

(a) D_1 = 0.5 mm, D_2 = 0.3 mm, D_3 = 0.5 mm, D_4 = 0.3 mm

(b) D_1 = 0.5 mm, D_2 = 0.3 mm, D_3 = 0.3 mm, D_4 = 0.5 mm

Fig. 11. Progressive deformation observed from three plates until the first and second contact obtained from specimens (5-i) and (5-ii), the gaps between plates being (a) (D_1, D_2, D_3, D_4) = (0.5 mm, 0.3 mm, 0.5 mm, 0.3 mm) and (b) (0.5 mm, 0.3 mm, 0.3 mm, 0.5 mm), respectively. Experimental results correspond well with the solid lines representing the analytical solution of Eq. (5).

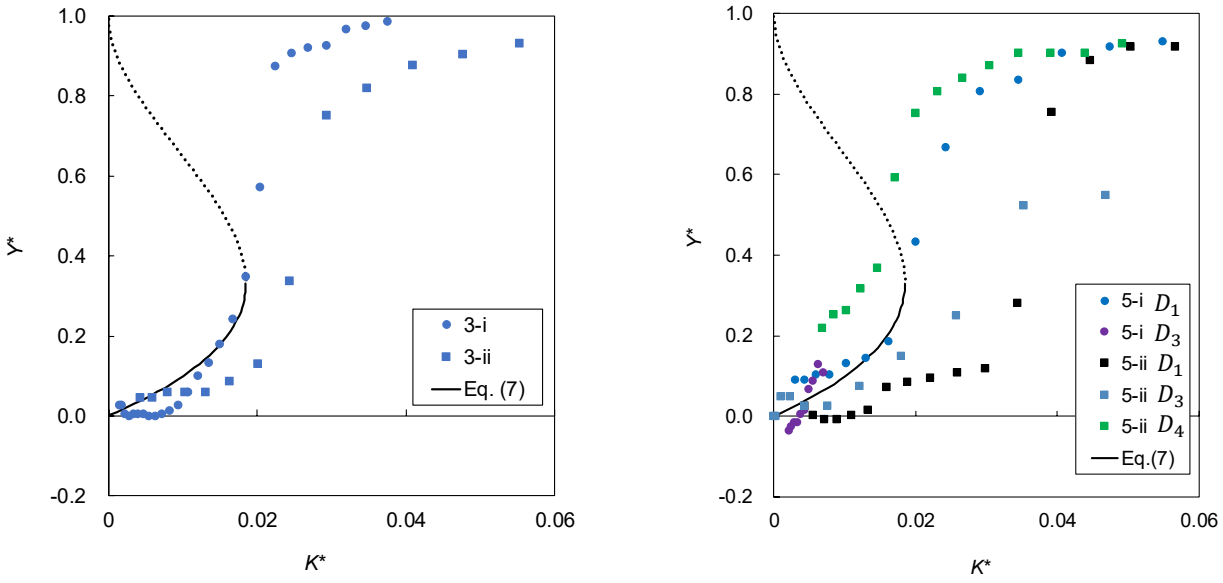

(a) Three plates

(b) Five plates

Fig. 12. Progressive deformation of three plates (a) and five plates (b) in terms of non-dimensional number *K**. The experimental results fall acceptably along the solid line representing the analytical solution when the aspect ratio *l*/*w* for the plate under liquid is sufficiently large compared with the capillary rise.